

ABC 11 - Program – DAY 2

Lecture theatre 505-011, Grafton Campus

4th Dec 2018

<p>9.00 am to 10.30 am</p> <p>Session Chairs:</p> <p>Prof Simo Saaraakala and A/Prof Egon Perilli</p>	<p>Invited Speaker - Dr Elizabeth Clarke University of Sydney/ Kolling Institute</p> <p>On: IN VIVO AND IN VITRO EXPERIMENTAL MODELS OF INJURY</p> <p>AWARDS SESSION I</p> <p>Scientific Presentations</p> <ul style="list-style-type: none"> • Wearable Sensors: Towards Evaluating Knee Joint Replacement Recovery – Shasha Yeung (University of Auckland) • Effect of neuromuscular exercise on joint contact forces in people following partial meniscectomy: secondary analysis of a randomised controlled trial – Scott Starkey (University of Melbourne) • Development of a virtual reality acetabulum reaming simulator and the need for biomechanical data - Mario Lorenz (Chemnitz University Of Technology) • The mechanical significance of the articular cartilage surface layer on tissue swelling. – Emma Brown (University of Auckland) <p>Imaging of structural and molecular transport compartmentalisation in an in vivo osteoarthritis model – Lucy Ngo (University of New South Wales)</p>
---	--

WEARABLE SENSORS: TOWARDS EVALUATING KNEE JOINT REPLACEMENT RECOVERY

Shasha Yeung¹, Jacob Munro², Ju Zhang¹, Thor Besier^{1,3}, Justin Fernandez^{1,3}

Auckland Bioengineering Institute
School of Medicine, University of Auckland
Engineering Science, University of Auckland

INTRODUCTION

The use of wearable technology has increased exponentially in clinical applications (Piwek, 2016). Coupled with patient motion analysis they have the potential to monitor and inform patient recovery following total knee joint replacement (TKR). This is beneficial for the health sector in monitoring patient recovery after surgery, especially orthopedics.

In this study we aim to (i) evaluate the use of small commercial inertial measurement units (IMUs) as a surrogate metric for knee joint loading following total knee joint replacement (TKJR), and (ii) give a quantitative measurement to the Oxford Knee Scoring metric used for evaluating degenerative knees.

METHOD

Twelve patients (age 69 ± 10 years; weight 105 ± 27 kg; height 151 ± 50 cm) were monitored from pre-surgery through to 6 weeks post-surgery recovery. Ethical approval was received from the University of Auckland human ethics committee (reference No. 015935).

A gait analysis, using a 9 camera Vicon system with split belt force plates, was conducted for each patient at baseline before surgery and after 6 weeks recovery collecting lower limb joint kinematics and kinetics. A Cleveland marker set was used (Figure 1 – right hand side). In parallel, IMU tibial accelerations were collected twice weekly. Wearable sensors were strapped on the anterior medial tibia site to minimize soft tissue artifacts (Figure 1). For each patient we correlated the peak tibial acceleration at heel strike, termed ‘tibial shock’, with their computed knee joint contact force (via a subject-specific scaled OpenSIM model) at baseline and after their recovery period. Throughout all time points, the Oxford Knee Scoring metric was used to evaluate the patient’s mood and overall pain levels. This was done as an online questionnaire to complement their sensor readings. The ‘tibial shock’ vs knee joint force was interpolated between these 2 time points to deduce the average knee joint loading as the patient recovered.

RESULTS

The IMU sensor revealed that most patients exhibited ‘tibial shock’ between 3Gs and 6Gs (30 m/s^2 to 60 m/s^2) at heel strike. Correlations between peak tibial acceleration at heel strike and knee joint force ranged from R^2 of 0.75 to 0.96 across all patients. This correlation changed between pre-surgery and post recovery for each patient. During each patient’s recovery timeline, some patients presented reduced peak ‘tibial shock’ while others maintained consistent peak ‘tibial shock’ before and after surgery. Their Oxford Knee Scoring results showed a general increased improvement over the recovery period and was similar in trend to the history of ‘tibial shock’ across 6 weeks.



Figure 1 - Sensor placement and marker set for gait analysis.

CONCLUSIONS

The study revealed that IMU wearables may act as a useful surrogate measure to predict knee joint force on a patient-specific level following TKJR. It also showed that the Oxford Knee Scoring is a useful measurement that mimics the ‘tibial shock’ trends during recovery.

REFERENCES

Piwek, L., Ellis, D. A., Andrews, S., & Joinson, A. (2016). The rise of consumer health wearables: promises and barriers. *PLoS Medicine*, 13(2), e1001953

Shasha Yeung

syeu670@aucklanduni.ac.nz

EFFECT OF NEUROMUSCULAR EXERCISE ON JOINT CONTACT FORCES IN PEOPLE FOLLOWING PARTIAL MENISCECTOMY: SECONDARY ANALYSIS OF A RANDOMISED CONTROLLED TRIAL

Scott Starkey¹, David Saxby², Gavin Lenton², Rana S Hinman¹, Tim Wrigley¹, David Lloyd², Kim Bennell¹, Michelle Hall¹

¹Centre for Health, Exercise, and Sports Medicine, University of Melbourne

²Innovations in Health Technology, Menzies Health Institute Queensland, Griffith University

INTRODUCTION

Following partial medial meniscectomy, people have a higher risk of developing knee osteoarthritis. Higher knee joint loads assessed via the external knee adduction moment have been related to structural disease progression in this population. Exercise is recommended for managing knee osteoarthritis symptoms, yet current evidence suggests that exercise does not alter knee joint loading [1]. However, no previous studies have accounted for the contribution of muscle activation in their estimates of knee load. This is important given the expected adaptations to muscle following exercise. Neuromuscular exercise is typically performed in functional weight-bearing positions, with an emphasis on neutral knee alignment, that may alter medial knee joint contact force.

The purpose of this analysis was to test the hypothesis that a 12-week neuromuscular exercise program would reduce medial knee joint contact force compared to no intervention. Secondary aims were to evaluate between-group differences in change in lateral and total knee joint contact forces and the relative muscle contributions to joint contact forces.

METHOD

This was a secondary analysis of data from a randomised controlled trial, where individuals aged 30-50 years with medial meniscectomy within the past 3-12 months, undertook either a 12-week neuromuscular exercise program or no intervention. The program included eight physiotherapist-supervised exercise sessions over a 12-week period, each lasting 30-40 minutes. Three home exercise sessions were also completed each week.

Participants' gait biomechanics were assessed in the lab at baseline and follow-up. While walking at a self-selected speed over ground, three-dimensional lower-body motion (Vicon, MX, Oxford, UK), ground reaction forces (AMTI Inc., Watertown, MA), and surface electromyograms (Noraxon, AZ, USA) from eight lower limb muscles were acquired from the affected limb. These data were used as inputs into an electromyogram-driven neuromusculoskeletal model [3], which estimated medial and lateral compartment

tibiofemoral contact forces (N), from which muscle and external load contributions (%) to these contact forces were determined.

RESULTS

41 (20/31 exercise, 21/31 control) out of 62 randomised participants had data suitable for analysis. Changes in knee joint contact forces (Table 1) and muscle contributions to joint contact forces (Figure 1) from baseline to follow-up were not significantly different between the groups.

Table 1. Between-group differences in changes in normalised knee joint contact forces (N/kg)

	Mean (95%CI)	p value
Peak lateral contact force	0.11 (-0.03, 0.24)	0.11
First peak medial contact force	0.12 (-0.08, 0.32)	0.24
Second peak medial contact force	0.10 (-0.07, 0.27)	0.26
First peak total contact force	0.17 (-0.09, 0.44)	0.19
Second peak total contact force	0.14 (-0.13, 0.42)	0.29

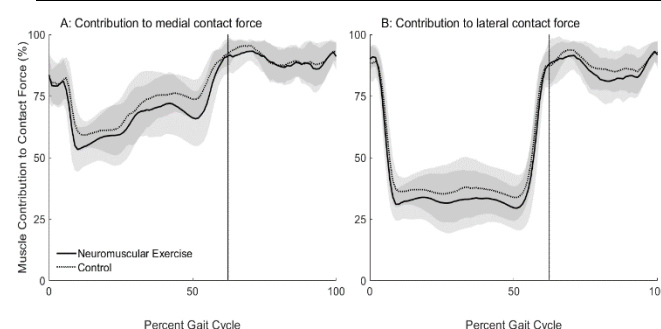


Figure 1. Muscle contributions (%) to medial and lateral contact force for both groups at follow-up.

CONCLUSIONS

These exploratory findings suggest that a 12-week neuromuscular exercise program may not reduce medial knee joint contact force in people following partial meniscectomy. However, this dataset was limited in its sample size due to quality of electromyogram data. Further research is needed to confirm whether exercise can alter knee joint contact force, a potential predictor of medial tibial structural damage.

REFERENCES

1. Ferreira, G et al. Clin Biomech 30(6), 521-7, 2015.
2. Hall, M et al. Med Sci Sports Ex 47(8), 1577-66, 2015.
3. Pizzolato C et al. J Biomech 48(14):3929-3936, 2015.

Mr. Scott Starkey
sstarkey@student.unimelb.edu.au

DEVELOPMENT OF A VIRTUAL REALITY ACETABULUM REAMING SIMULATOR AND THE NEED FOR BIOMECHANICAL DATA

Mario Lorenz^{1,2}, Sebastian Knopp¹, Luigi Pelliccia¹ Niels Hammer^{2,3}

¹Chemnitz University of Technology; Professorship for Machine Tools and Forming Technology

²University Clinics of Leipzig; Department of Orthopedics, Trauma and Plastic Surgery

³University of Otago; Department of Anatomy, Clinical Anatomy Research Group

INTRODUCTION

Virtual Reality (VR) is a powerful tool with application areas reaching from entertainment to training. Especially for the training of surgeons, VR can be a powerful addition to traditional training methods. Training surgeons in VR is riskless and can at the same time save precious resources like human cadavers or living animal stock, which would otherwise be used for training. Arthroscopic or laparoscopic VR training simulators are impressive examples of the achievable benefits (Escobar-Castillejos et al., 2016). However, such minimally invasive operations are niche applications considering the overall number of operations, especially in orthopedics and trauma. Just primary hip replacements are performed several hundred thousand times per year worldwide. Yet, we fail to see according surgical VR training simulators. The two reasons for this are the high forces, which need to be simulated, and the lack of biomechanical data to develop fast computing material models needed for haptic simulation. In the given project entitled HIPS, we tackled both challenges and developed a surgical VR simulator for the reaming procedure of the acetabulum in the course of primary hip replacement (Kaluschke et al., 2018).

METHOD

We utilized an industrial collaborative KUKA iiwa robot with a capacity of 14 kg as a haptic force feedback device to simulate the applied forces. The HTC VIVE was used as a VR goggle to show the virtual operation scene and Unity3D as a VR software. The patients' anatomy was generated with the 3D modeling software Blender. A fast computing collision and material removal algorithm ensured reliable haptic behavior (Kaluschke et al., 2018). The data gathered from biomechanical tests with 24 human acetabuli formed the basis for a fast computing material model.

RESULTS

Figure 1 shows the prototype of the developed VR acetabulum reaming simulator. We developed a control algorithm, which allowed us to utilize the KUKA iiwa robot as a haptic force feedback device and at the same time preserve the built-in security functionalities (Knopp et al., 2018). The biomechanical tests revealed that forces up to 150 N need to be simulated, which the KUKA iiwa robot is capable of. A fast computing

spline-based material model was developed from the filtered biomechanical data. It was implemented to simulate the haptic force feedback for the acetabulum reaming. A seamless integration of the VR training scene, the haptic force feedback and the material removal simulation was achieved. A preliminary consultation of surgeons confirmed an overall realistic visual simulation. Currently outstanding are user tests with experienced surgeons to validate especially the correct haptic behavior. The evaluation of the haptic simulation may form the basis for further optimization.



Figure 1. HIPS –VR acetabulum reaming simulator. In the front the KUKA iiwa robot can be seen with an attached hip reaming device. In the back the screen shows the progress and success in VR training scene.

CONCLUSIONS

We built the world's first surgical VR training simulator for non-minimally invasive surgery using an industrial robot as a haptic force feedback device. Biomechanical tests formed the baseline data for a material model to achieve a realistic haptic feeling.

ACKNOWLEDGEMENTS

The German Federal Ministry of Economic Affairs and Energy (16KN036255) funded this work.



REFERENCES

- Escobar-Castillejos, D., et al. J. of Medical Systems 40, 104, 2016.
- Kaluschke, M., et al. Proceedings of IEEE VR 2018. (in print)
- Knopp, S., et al. Proceedings of IEEE VR 2018. (in print)

Speaker: Mario Lorenz

mario.lorenz@mb.tu-chemnitz.de

THE MECHANICAL SIGNIFICANCE OF THE ARTICULAR CARTILAGE SURFACE LAYER ON TISSUE SWELLING

Emma Brown, Alicia Damen, Neil Broom, Ashvin Thambyah

1) Experimental Tissue Mechanics Laboratory, Department of Chemical & Materials Engineering, The University of Auckland

INTRODUCTION

When excised from the underlying bone, articular cartilage has been observed to curve (or arch), with this curvature tending to be emphasized when the tissue is exposed to an osmotic solution (1). This previous work, from the renowned Mow group suggests that the curvature is due to the fixed charge density differential from the surface layer to the deep zone of cartilage and/or matrix anisotropy. Within the surface layer are densely packed tangentially-aligned collagen fibrils which, may be responsible for restricting deformation relative to the deep zone, causing the tissue to curve. The present research considers such curving behavior of free articular cartilage swelling, from a structural standpoint, and with particular regard to the mechanical significance of the strain-limiting surface layer.

METHOD

Approximate full-thickness (~ 2mm) strips of pristine appearing articular cartilage were harvested from young adult bovine patellae cartilage-on-bone blocks. Each strip measured approximately 2mm wide and 12 mm long. Four individual sample strips per block, two with surface layer intact and two with surface layer removed, were obtained. Surface layer removal was carried out using a sledging microtome set at 200 μ m thickness. A total of 26 cartilage blocks were used, yielding 108 strips for the testing.

Each strip was exposed to a 0.15M saline solution for approximately 3 hours followed by a final distilled water solution equilibration for an additional three hours. Each strip was imaged immediately upon removal from the bone as well as after each fluid equilibration step. Image J software was used to quantify dimensional changes of each strip at each testing step. Following imaging, the strips were chemically-fixed, sliced into 30 micron sections and imaged by differential interference contrast microscopy (DIC) to examine the tissue structural detail.

RESULTS

There was a large variation in the swelling response. However each final swelling (deformation) response could be categorized into one of a total six possible shape categories (Figure 1). Approximately 40% of all samples remained straight and of these approximately half were intact while the other had their surface layer

removed.

Of the specimens that adopted an arch morphology, approximately 85% had an intact surface layer. This tends to support the aforementioned strain-limiting properties of the articular surface layer and its contribution to the curling response. However this is not sufficient to explain the full range of deformation morphologies observed. DIC micro-imaging revealed that the extent to which the very deep zone cartilage tissue was included in the strips may be a possible influencing factor in the varied deformation outcomes displayed. More work looking into the micro-to-nano scale fibrillar structure will be carried as a result of this insight, that the very deep zone cartilage is also relatively strain-limiting.

	Arch	Bend	Spiral	Straight	Twist	Wave	Total
WO	2	11	6	19	2	12	52
W	11	10	5	21	5	0	52
Total	13	21	11	40	7	12	104

Table 1: Count of final shape configuration following distilled water equilibration for samples with surface layer intact (W) and those without (WO).

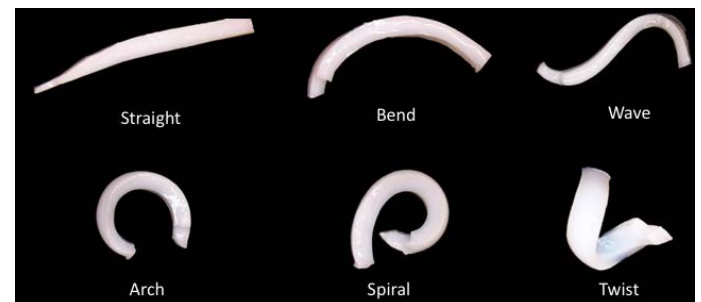


Figure 1: Six different shape categories

CONCLUSIONS

A relatively large number of deformation responses are possible from cartilage swelling, challenging our expectations of how the different zones are involved in cartilage mechanics, and our assumptions of transverse isotropy.

References

- (1) J Biomech Eng 120, 355-361, 1998
Speaker: Emma Brown
Email: emma.brown@auckland.ac.nz

IMAGING OF STRUCTURAL AND MOLECULAR TRANSPORT COMPARTMENTALISATION IN AN IN VIVO OA MODEL

Lucy Ngo¹, Melissa L. Knothe¹

Graduate School of Biomedical Engineering, UNSW Sydney, Australia

INTRODUCTION

Osteoarthritis (OA) is resultant of complex interactions between tissues of the entire joint underpinned by multifactorial processes of disease structure and function degeneration. Understanding progressive disruptions to molecular transport may have important implications for deciphering OA aetiology and pathogenesis. Multimodal imaging facilitates dissection of interactions across length-scales. This study explores transport through joint tissue dependent on molecular size-selectivity and boundary membrane functional barrier properties.

METHOD

Dunkin-Hartley guinea pigs (DHGP) are an animal model for spontaneous, age-related knee OA. DHGP exhibit OA pathology comparable to humans; extending to the molecular level, quantifiable with biomarkers and histology¹. A single mixed-bolus of neutral fluorescent-tagged-dextran, 70kDa (red) and 10kDa (green) injected via the heart into two anaesthetized cohorts, comprising of 8-10-month and 17-19-month animals. The young and old cohort corresponded approximately to middle-aged and aged humans, respectively. After five minutes' circulation animals were euthanised, knees resected and left knees cryo-fixed, followed by serial-episcopic blockface fluorescence imaging (CryoViz, BioInVision, USA). Contralateral specimens, polymethylmethacrylate embedded, were imaged with fluorescent confocal microscopy (Leica SP5 II, Germany).

RESULTS

Blockface imaging showed size-based tracer separation in anaesthetized animal tissue compartments. Young joints exhibited significantly greater green tracer concentrations than aged. Tracer was absent in boundary tissues including the growth plate, periosteum and cartilage. Confocal microscopy enabled high resolution imaging of structure and functional

characteristics i.e. trabecular surface osteoclastic activity.

Confocal microscopy confirmed red tracer in the marrow space and revealed small, round red aggregations distributed in proximity to marrow vasculature (Fig 1B). Also confirmed was macromolecular transport across cartilage and through the subchondral plate, with strongest tracer signal in channels observed to traverse between cartilage surface to subchondral plate (Fig 1C, D).

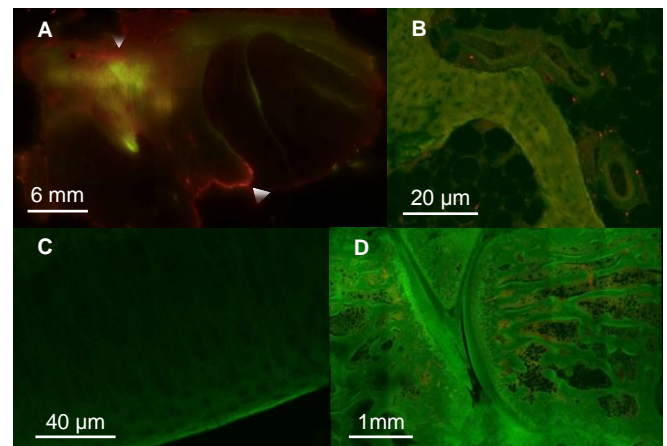


Figure 1A. Episcopic blockface image of muscle showed fluorescence limited to bounding fasciae. B, C, D. Confocal images illustrating round aggregations of red tracer transport channels across cartilage and tracer delineation of tissues, respectively.

CONCLUSIONS

Molecular communication is implicated as a potential factor in OA pathophysiology. Further imaging using additional modalities such as EM may facilitate greater understanding. This may aid to slow joint tissue degradation progression and modulate joint health by harnessing spatiotemporal transport mechanisms.

REFERENCES

1. Ngo et al. Nat. Sci. Reports. 2018 [In press]

Speaker: Lucy Ngo Email: lucy.ngo@unsw.edu.au

ABC 11 - Program – DAY 2

Lecture theatre 505-011, Grafton Campus

4th Dec 2018

<p>11.00 am to 12.45 pm</p> <p>Session Chairs:</p> <p>A/Prof Justin Fernandez and Prof Rami Korhonen</p>	<p>Invited Speaker - Professor Neil Broom</p> <p>University of Auckland</p> <p>On: EXPLORING SOFT-HARD JUNCTIONS IN THE MUSCULOSKELETAL SYSTEM: AN EXPERIMENTAL APPROACH</p> <p>AWARDS SESSION II</p> <p>Scientific Presentations</p> <ul style="list-style-type: none"> • Structural Integration Across the Endplate Cement Line - Nurul Haiza (Zaza) Sapiee (University of Auckland) • Muscle architecture in the medial gastrocnemius of stroke patients: a diffusion tensor imaging investigation – Arkiev D'Souza (Neuroscience Research Australia) • Sub-critical knee injury: a risk factor for critical injury and osteoarthritis in mice - Carina Blaker (University of Sydney) • Speed-adaptive myoelectric ankle exoskeleton to improve post-stroke walking performance – Taylor Dick (University of Queensland) • Assessment of thorax and rib cage joint rigidity on spinal loading - Hossein Mokhtarzadeh (Harvard Medical School) <p>Pericellular matrix thickness distribution around chondrocytes is orientation-dependent - Eng Kuan Moo (University of Calgary)</p>
--	--

STRUCTURAL INTEGRATION ACROSS THE ENDPLATE CEMENT LINE

Nurul Haiza Sapiee¹, Ashvin Thambyah¹, Peter Roberston², Neil Broom¹.

1. Experimental Tissue Mechanics Laboratory, The University of Auckland, New Zealand
2. Department of Orthopaedic Surgery, Auckland City Hospital, New Zealand

INTRODUCTION

A recent biomechanical study of the endplate region in human thoracic spines showed a greater incidence of failure at the cement line, the junction between the cartilaginous endplate (CEP) and vertebral endplate (VEP) [1]. It has been suggested that this junction has poor structural connectivity giving rise to an increased vulnerability to avulsion of the CEP from the VEP [1]. However, in herniated disc material, both cartilaginous and osseous material from the endplate are often present suggesting that failure at the endplate can involve both the CEP and VEP [2]. The mechanical significance of the organic and mineral phases in the endplate thus requires further exploration, especially concerning how these influence endplate strength and its modes of failure.

Employing site-specific decalcification in combination with a partial rupture technique, this study investigated how integration is achieved across the cement line of mature ovine lumbar discs at the micro- and ultra-structural levels.

METHODS

Vertebra-annulus-vertebra samples (n=33), ~5mm x 6mm in cross-section, were prepared from the anterior and posterior regions of 25 mature ovine lumbar motion segments such that the lamellar fibres in one of the oblique fibre directions extended from vertebra to vertebra. The samples were then subjected to site-specific decalcification confined to the region of the endplate and then stretched axially to an extent sufficient to achieve partial rupture of the endplate region. The failure regions were analysed using both differential interference contrast microscopy (DIC) and scanning electron microscopy (SEM).

RESULTS

Microstructural analysis revealed that failure in tension in the endplate region was not confined to the cement line alone. Instead, partial tears continued into the underlying vertebral endplate with bony osteon material still attached to the annular bundles (Fig.1).

Ultrastructural analysis of the ruptured regions of the cement line revealed clear evidence of blending/interweaving relationships between the fibrils of the annular bundles, the calcified cartilage and the bone with no one pattern of association appearing dominant.

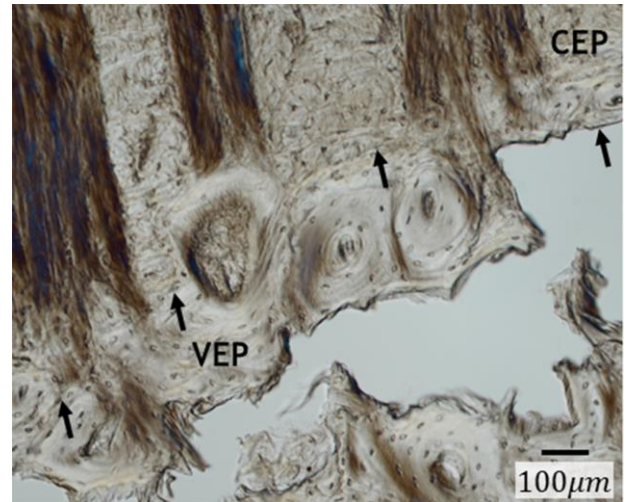


Fig. 1: Evidence of osseous vertebral material still attached to the detached annulus/CEP. Arrows indicate cement line.

Variable patterns of association of the fibrils combined with clear evidence that the cement line is not a preferred plane of weakness even following decalcification suggest fibril-based structural cohesion exists at the cement line. Our data show integration across this junction with strengthening via a mechanism analogous to how the strength in a steel-reinforced concrete structure is achieved. The steel elements are brought into a close intermingling association and the concrete matrix provides that all-important integrating medium. This, we suggest, parallels the role of end-plate junction mineralisation.

CONCLUSIONS

This study provides clear evidence of structural connectivity across the endplate cement line via the intermingling of their fibrillar components and mediated by the mineral phase. This is consistent with clinical evidence showing that in some disc herniations the extruded soft tissue can include still-attached osseous material.

ACKNOWLEDGEMENTS

The first author gratefully acknowledges Medtronic Australasia for funding her doctoral scholarship.

REFERENCES

- [1] Berg-Johansen B, et al. J Ortho. Re. 36, 1-10, 2017.
- [2] Rajasekaran S, et al. Spine 38, 1491-1500, 2013.

Speaker: Nurul Haiza Sapiee

Email: nsap465@aucklanduni.ac.nz

MUSCLE ARCHITECTURE IN THE MEDIAL GASTROCNEMIUS OF STROKE PATIENTS: A DIFFUSION TENSOR IMAGING INVESTIGATION

Arkiev D'Souza, Bart Bolsterlee, Rob Herbert

Neuroscience Research Australia and University of New South Wales, Sydney, Australia

INTRODUCTION

Muscle contracture is a loss in joint range of motion caused by increases in the passive stiffness of muscles. Contractures commonly occur in patients who have had a stroke, and frequently occur in the ankle [1]. Ankle contractures compromise balance and mobility. No effective treatment for contracture currently exists, and the underlying mechanisms of contracture are poorly understood. This work investigates changes in muscle architecture in the medial gastrocnemius of people who have contracture after stroke.

METHOD

Muscle architecture of the medial gastrocnemius was measured in 12 stroke patients (age 60 ± 13 years; mean \pm SD) and 17 control subjects (age 66 ± 12 years; mean \pm SD) using diffusion tensor imaging (DTI). The lower legs were scanned in a 3T MRI scanner (Philips Achieva TX) while lying supine. The scan protocol consisted of an mDixon and a DTI scan. The mDixon scan was used to measure muscle volume. Using DTI tractography, three-dimensional fascicle lengths, pennation angles, physiological cross-sectional area (PCSA) and fascicle curvatures were measured [2]. Dorsiflexion range of motion was measured when 10 Nm was applied to the ankle. For control subjects, the mean measurements of the left and right muscle were used. Linear mixed models compared muscle architecture and dorsiflexion range of motion between (1) the paretic and non-paretic sides from stroke patients, (2) the paretic side of stroke patients and control subjects, and (3) the non-paretic side of stroke patients with control subjects

RESULTS

In the stroke patients, the paretic side had 10° less range of motion (95% confidence interval 7° to 13°) and 44cm^3 (5cm^3 to 83cm^3) smaller muscle volume than the non-paretic side (Figure 1). The paretic side had 6° (0° to 13°) less dorsiflexion and 13cm^2 (3cm^2 to 24cm^2) smaller PCSA than the control subjects. We did not detect any differences between the non-paretic side and control subjects. In addition, we did not detect a significant difference in fascicle length or pennation angle in either of the three comparisons.

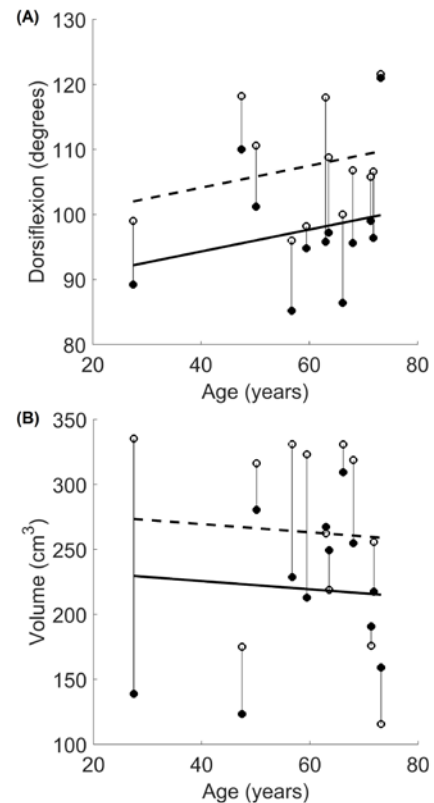


Figure 1: Ankle dorsiflexion range of motion (A) and muscle volume (B) on the paretic and non-paretic side of stroke patients. Filled circles are the measurements from the paretic side and open circles are measurements from the non-paretic side. Vertical lines join measurements from the same subject. The solid and dashed lines are regression lines for the paretic and non-paretic side, respectively.

CONCLUSIONS

DTI-based, three-dimensional measurements of muscle architecture were obtained from the medial gastrocnemius muscles of stroke patients and controls. The paretic side showed a large reduction in dorsiflexion range of motion and reductions in muscle volume and PCSA. In this work in progress, we did not detect any changes in fascicle length or pennation angle.

REFERENCES

- [1] Kwah, K., J Physiotherapy, 58, 41-47, 2012
- [2] Bolsterlee, B., J Appl Physiol, 122, 727-738, 2017

Contact: Arkiev D'Souza (a.dsouza@neura.edu.au)

SUB-CRITICAL KNEE INJURY: A RISK FACTOR FOR CRITICAL INJURY AND OSTEOARTHRITIS IN MICE

Carina Blaker^{1,2}, Sanaa Zaki², Christopher Little² and Elizabeth Clarke¹

¹Murray Maxwell Biomechanics Laboratory and ²Raymond Purves Bone and Joint Research Laboratories, Institute of Bone and Joint Research, Kolling Institute, Northern Sydney Local Health District, Sydney Medical School Northern, University of Sydney, St. Leonards, NSW, Australia

INTRODUCTION

The incidence of anterior cruciate ligament (ACL) tears is increasing at a substantial rate¹ and has considerable long-term consequences with 1 in 2 patients at risk of developing osteoarthritis (OA) within 10-20 years of injury². Current prevention strategies seek to modify aberrant motions which cause excessive loading of the joint but do not yet address factors which may actively reduce the threshold for critical injury. Prior injuries are known to increase the likelihood of subsequent injuries and there is evidence to suggest that elevated markers of ligament and cartilage remodelling are predictive of patients at risk of ACL injury³. This suggests that prior sub-critical injuries may play a role in increasing ACL rupture risk and susceptibility to OA development after critical injury. To investigate this hypothesis, we evaluated the effects of a sub-critical knee injury in mice.

METHOD

A single compressive load was applied to the right knee of 10-week-old male C57BL/6 mice to induce a sub-critical injury at approximately 70-80% of the mechanical load required to induce an ACL tear. Outcomes were assessed at 1, 2, 4 and 8 weeks post-injury and compared to un-injured controls. Pain responses were measured longitudinally by static weight-bearing or mechanical allodynia (n=6/group). Anterior-posterior knee mechanics (range of motion and joint stiffness, n=6/group) and changes in ACL strength (n=8/group) were measured ex vivo. Joint pathology including cartilage damage and subchondral bone changes were evaluated histologically in the medial and lateral tibiofemoral compartments, and the patellofemoral compartment (n=7/group).

RESULTS

Although sub-critical knee injury did not cause unloading of the injured limb in a static standing position there was evidence of significant allodynia from 1-8 weeks post-injury ($P<0.0001$). Mechanically, sub-critical knee injury had no effect on anterior-posterior joint laxity but was found to significantly impact ACL strength ($P=0.0148$, Figure 1A). At 4 and

8 weeks post-injury ACL strength was reduced by 14-16% compared to un-injured controls. Sub-critical injury also induced focal lesions in both the cartilage and subchondral bone of the patella and lateral tibial plateau (Figure 1B). These lesions were present from 1-8 weeks post-injury ($P\leq 0.0363$) but did progress over time.

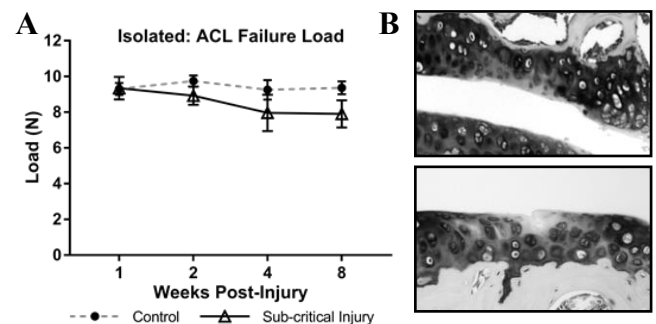


Figure 1. Sub-critical knee injury causes (A) reduced ACL strength over time (mean \pm SEM) and (B) focal cartilage lesions in the patella (upper image) and lateral tibial plateau (lower image).

CONCLUSIONS

A single sub-critical knee injury caused significant reduction in the failure load of the ACL indicating an increased predisposition to ACL tears compared to un-injured joints. This reduction could not be predicted by measures of joint laxity or pain indicated by weight-bearing on the injured limb but may be related to increased sensitisation to mechanical stimuli (allodynia). The injury induced focal lesions observed in the cartilage and bone may not be progressive but this initial disruption to tissue integrity will increase susceptibility to subsequent injuries and OA progression. These results highlight the importance of acknowledging and addressing sub-critical injuries as risk factors for both critical injury and OA.

REFERENCES

- Zbrojkiewicz, D. Med J Aust. 208, 354-368, 2018.
- Lohmander, L. Am J Sports Med. 35, 1756-1769, 2007.
- Svoboda, S. J. Am J Sports Med. 44, 1687-1693, 2016.
- Speaker: Carina Blaker (carina.blaker@sydney.edu.au)

SPEED-ADAPTIVE MYOELECTRIC ANKLE EXOSKELETON TO IMPROVE POST-STROKE WALKING PERFORMANCE

¹Taylor JM Dick, ²Emily M McCain, ²Tracy N Giest, and ³Gregory S Sawicki

¹University of Queensland, St Lucia, QLD, Australia

²North Carolina State University, Raleigh, NC, USA

³Georgia Institute of Technology, Atlanta, Georgia, USA

INTRODUCTION

Limited ankle ‘push-off’ power is a hallmark of post-stroke gait, leading to high inter-limb asymmetry, reduced walking speeds, and elevated metabolic demands [1]. Powered wearable robotic exoskeletons offer a promising approach to restore these mechanical deficits by applying torque at the paretic ankle during the propulsive phase of walking.

Previous devices [2] have been effective at improving paretic ankle plantarflexion moment during walking, but were unable to increase ankle power output or reduce the metabolic costs of paretic gait. This particular devices’ performance was limited because: (i) it was unable to respond to reductions in plantarflexor muscle activity that occur with added assistance and (ii) the subjects’ walked at slow speeds where assistance was not needed. In this study, we extend previous work by developing and testing a novel powered ankle exoskeleton – driven with the user’s soleus electromyographic signal and ground reaction force profile—that modulates propulsive assistance with walking speed and ensures assistance levels do not decline with reductions in muscle activity.

METHODS

We implemented a speed-adaptive controller designed to mitigate the specific limitations of prior controllers. The controller used real-time soleus muscle activity [3] and a speed-dependent gain to ensure a torque profile of ~25% of the maximum healthy ankle plantarflexion moment at a particular treadmill speed. The exoskeleton torque profile was applied by a benchtop motor to the carbon-fiber device via a Bowden-cable transmission system. Experimental data was collected from six stroke

survivors walking on an instrumented split-belt treadmill with and without an exoskeleton on their paretic limb. Subjects started by walking at 60% of their preferred speed (n00) in a speed-endurance test whereby at each consecutive minute, treadmill speed increased by 0.1 m s^{-1} . We collected kinematics, kinetics, surface electromyography, and metabolic cost. Inverse dynamics was used to determine joint moments. Joint powers were calculated for the ankle, knee, and hip. Statistical significance of peak and net ankle power was determined using paired t-tests ($\alpha=0.05$).

RESULTS

The exoskeleton was able to increase assistive torque as walking speed increased and muscle activity decreased, verifying its efficacy (Fig. 1c). At all walking speeds, peak and net paretic ankle power were significantly higher when the participants wore the exoskeleton compared to normal walking (Fig 1a/b). Despite the improvement in ankle function, only 2 of the 6 subjects experienced a reduction in metabolic cost while wearing the device.

CONCLUSIONS

This study suggests that assistive devices have the potential to restore paretic ankle function in post-stroke individuals, however future work into the proximal joint-level effects of added assistance is necessary.

REFERENCES

- [1] Peterson, CL et al. *J Biomech.* 2010; 43:2348–55
- [2] Takahashi, KZ et al. *J NeuroEng Rehab.* 2015; 12:23
- [3] Koller, JR et al. *J NeuroEng Rehab* 2015; 12:97

Speaker name: Taylor Dick t.dick@uq.edu.au

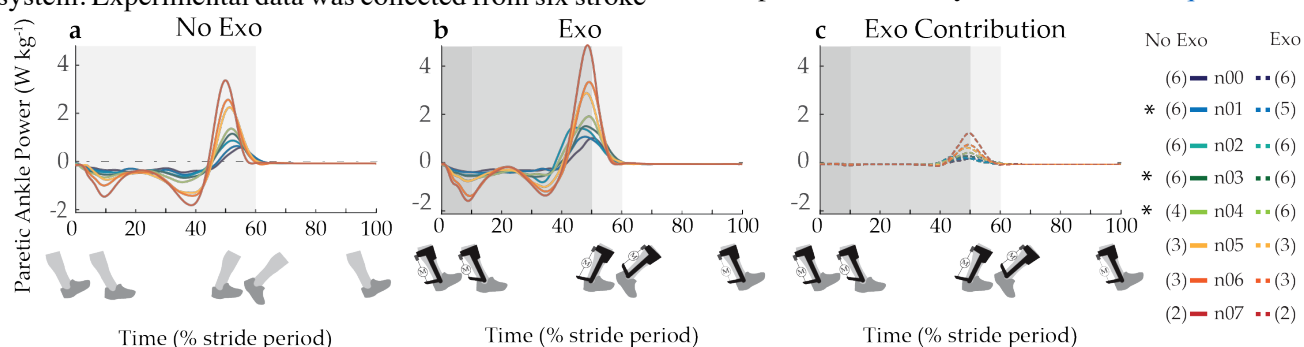


Fig. 1 (a) Paretic ankle power in the no exoskeleton (exo) condition and (b) the exo condition with the (c) exo contribution isolated. The number of subjects is indicated in parenthesis. The shaded area represents stance.

ASSESSMENT OF THORAX AND RIB CAGE JOINT RIGIDITY ON SPINAL LOADING

Hossein Mokhtarzadeh^{1,2}, Dennis Anderson^{1,2}, Mary Bouxsein^{1,2}

¹Harvard Medical School, Boston, USA. ²Beth Israel Deaconess Medical Center, Boston, USA

INTRODUCTION

Spinal curvature including thoracic kyphosis angles alters with aging, and excessive curvature is associated with a variety of functional and health problems. We have previously shown that estimates of spinal loading are sensitive to individual variations in spine curvature [1]. Aging may also reduce the mobility of the thorax, which may reflect increased stiffness or rigidity of thoracic intervertebral or costovertebral joints, but the influence of joint stiffness on thoracic spine loading remains unexplored. Thus, we performed a preliminary study of the effect of joint rigidity in the thorax and rib cage on spinal compressive loading. This work in addition to our previous work has been appeared in recent WCB2018 conference*.

METHOD

We used a thoracolumbar spine model with rib cage in OpenSim, validated for calculating thoracolumbar spine loading [2]. The model includes costovertebral and intervertebral joints with one and three degrees of freedom, respectively. We considered four scenarios of varying joint rigidity: a) baseline, all joints free to move, b) locking only the costovertebral joints connecting the ribs to vertebrae (ribs fixed), c) locking only thoracic intervertebral joints (thorax fixed), d) locking both thoracic intervertebral and costovertebral joints (thorax and ribs fixed). These models were solved for muscle redundancy in four loading conditions using static optimization in OpenSim. Thoracolumbar spine loading was predicted based on muscle forces at each posture.

RESULTS

Introduction of joint rigidity produced large differences in spin loading from the baseline case, although varying widely across activities and spinal regions. For example, spine loading increased by up to 25% during 30° trunk flexion with 10 kg weights in each hand (Figure). Across the activities, the fixed rib cage tended to increase loading in the upper thoracic spine, but had less effect at lower spine levels. Conversely, the fixed thorax tended to reduce forces in upper thoracic regions (T1-T7), but increase forces in lower spinal regions.

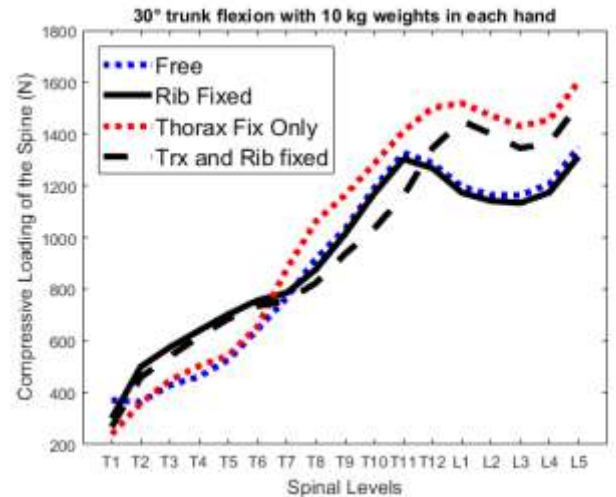


Figure 1. Spine compressive loading (N) by level for 30deg trunk flexion with 10kg load in each hand.

CONCLUSIONS

These results show that rigidity of the thorax and rib cage joints strongly influences estimated spinal loading. As we have shown before, spinal loading is sensitive to subject-specific curvature and muscle morphology [1]. This preliminary study suggests that variations in joint stiffness could have as much of an effect as curvature on spine loading, and provides motivation to examine the effects of joint stiffness on spine loading more closely in future studies. Incorporating realistic and ultimately subject-specific estimates of spine and rib cage stiffness into models estimating spinal loading may be important for better understanding of the biomechanical and clinical effects of aging and spinal conditions.

Acknowledgments: This work was supported by the US National Institutes of Health (R01AR053986).

REFERENCES:

- [1] Bruno AG, et al., J Orthop Res, 35(10):2164-2173, 2017.
- [2] Bruno AG, et al., J Biomech Eng, 137:81003, 2015.

Speaker: Dr. Hossein Mokhtarzadeh,

Mokhtarzadeh.hossein@gmail.com

- This abstract has also been published and presented in 8th World Congress of Biomechanics (WCB2018).

PERICELLULAR MATRIX THICKNESS DISTRIBUTION AROUND CHONDROCYTES IS ORIENTATION-DEPENDENT

¹Eng Kuan Moo, ¹Scott C. Sibole, ¹Walter Herzog.

¹Human Performance Laboratory, Faculty of Kinesiology, University of Calgary, Canada

INTRODUCTION

Articular chondrocytes are surrounded by a thin layer of pericellular matrix (PCM) that is mechanically and biochemically distinct from the surrounding extracellular matrix (ECM) [1, 2]. This thin layer of PCM has been thought to play crucial roles in macro-molecular transport and transmission of mechanical deformation between the ECM and cells [1-3]. Mechanically, the PCM is thought to be protective of cells during loading, and has been modelled as a layer of uniform thickness around cells [4]. However, the PCM has been shown to have non-uniform thickness around cells [2, 5]. It is not understood how this geometrical variation of PCM thickness affects force transmission from the ECM to the cell, and if the PCM thickness distribution is dependent on the orientation of the cell. The purpose of this study was to quantify the *in situ* thickness of the PCM as a function of cell orientation.

METHOD

Lapine cartilage-bone explants (N=2) were harvested from the femoral groove. The cartilage was stained with 5-DTAF (for ECM, Ex: 492nm, Em: 516nm) and Calcein Red/Orange AM (for live cell, Ex: 577nm, Em: 590nm) for 1h. The top 100µm of the tissue was imaged using multi-photon laser microscopy. As 5-DTAF only labels the ECM up to the boundary of the chondron (cell & PCM), the PCM can be visualized as the unstained dark region from the resulting image merged from the ECM and live cells (Fig. 1A). The PCM thickness is defined as the perpendicular distance between the cell and the chondron at every point on the cell surface (Fig. 1B). In order to correlate PCM thickness to cell orientation, the PCM thicknesses were divided into three regions: top, bottom and side, based on the polar angle of the cell relative to the articular surface (Fig. 1B, bottom right). The mean regional difference in PCM thickness was compared using Mann-Whitney U test.

RESULTS

A total of 23 cells were analyzed. The bottom region facing the bone was thicker than both the top and side regions. There is no difference between the top and the side regions (Fig. 1C).

CONCLUSIONS

Our preliminary results suggest that the PCM thickness distribution is orientation-dependent, with the bottom region being thicker than the side and the top regions. Considering that the elastic modulus of the PCM is uniform around the cell [5], such distribution of thickness may affect the force transmission from the extracellular matrix to the cells, and warrant further investigation in the near future.

REFERENCES

[1] Guilak et al. Ann N Y Acad Sci 2006; [2] Choi et al. J Biomech 2007; [3] Wilusz et al. Matrix Biol 2014; [4] Guo and Torzili Acta Biomaterialia 2017; [5] Wilusz et al. J Roy Soc Int 2012

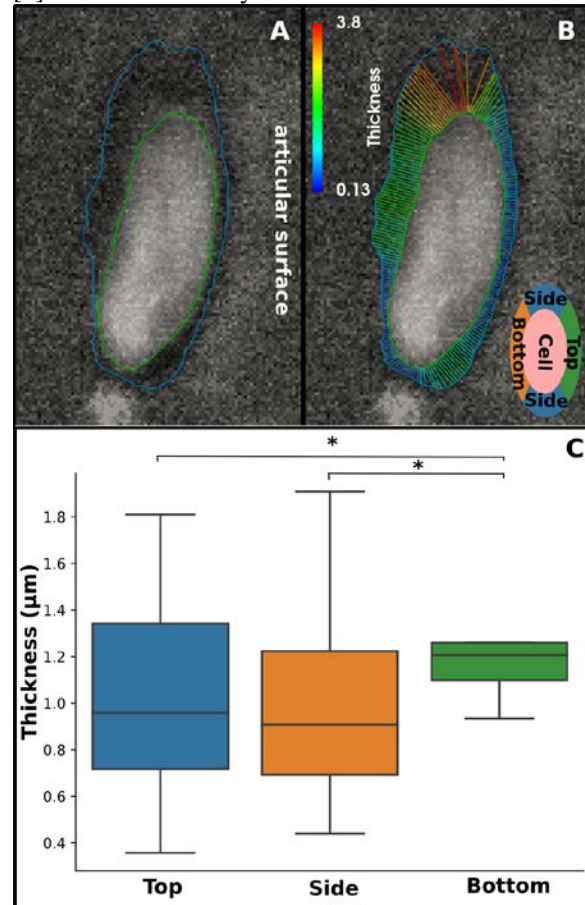


Fig. 1. (A) Representative image of a chondron containing a single cell (green outline) labelled by dual staining of the ECM and live cells. (B) the PCM thickness distribution around the cell, (C) variation of PCM thickness at the top, bottom, and side of the cell. * – difference is statistically significant ($p < 0.01$)

ABC 11 - Program – DAY 2

Lecture theatre 505-011, Grafton Campus

4th Dec 2018

<p>1.30 pm to 3.00 pm</p> <p>Session Chairs: Dr Vickie Shim and Dr Marcos Domingos</p>	<p>COMPUTATIONAL MODELING I</p> <p>Invited Speaker - Professor Tim David University of Canterbury</p> <p>On: PARALLEL INTEGRATED MODELS OF NEUROVASCULAR COUPLING AND BOLD SIGNALS</p> <p>Scientific Presentations</p> <ul style="list-style-type: none"> • Effects of pth treatment in osteoporosis – insights from a mechanistic pk-pd model - Maxence Lavaill (Queensland University of Technology) • Can humeral fractures occur spontaneously in infant while rolling? A finite element study - Zainab Altai (University of Sheffield) • Time-course changes of lower limb kinematics during military load-carriage - Jodie Wills (Macquarie University) • Development of a deep neural network for automated electromyographic pattern classification – Riad Akhundov (Griffith University and University of Newcastle) <p>Hip arthokinematics determined using subject-specific mri and mesh contact theory – David Saxby (Griffith University)</p>
--	---

EFFECTS OF PTH TREATMENT IN OSTEOPOROSIS – INSIGHTS FROM A MECHANISTIC PK-PD MODEL.

Maxence Lavaill^{1,4}, Silvia Trichilo², Stefan Scheiner³, Peter Pivonka⁴

¹ Queensland University of Technology, Australia; ² University of Melbourne, Australia; ³ Vienna University of Technology, Austria; ⁴ Universite de Technologie de Compiegne, France

INTRODUCTION

Osteoporosis (OP) is a common age- and sex- related disease which can cause bone fractures. The currently only available and approved anabolic treatment for OP is daily injections of PTH (1-34). This drug has a specific dual action, i.e. it can act either anabolically or catabolically depending on the type of drug administration (intermittent or continuous). Few models have tried to simulate these actions on bone modeling and remodeling in animal models ^a. However, the latter model does not incorporate mechanobiological feedback which is important for the action of PTH in human bone remodeling. Hence, in this study, we aim to develop a mechanistic pharmacokinetic-pharmacodynamic (PK/PD) model of the action of PTH (1-34) in postmenopausal osteoporosis (PMO). This will help to obtain a better understanding of the effect of different treatment patterns on bone mineral density (BMD). Accounting for mechanical feedback in the model allows simulating the effect of bone mechanical disuse as occurs in the aging population on BMD.

METHOD

A bone cell population model coupled with a micromechanical model of bone stiffness is used to compute changes of the BMD within a representative volume element ^b. The latter model has a characteristic time scale of weeks to months. The PK model of PTH (1-34) used in this study is a one-compartment model and has a characteristic timescale of hours. Concentration of PTH in the central compartment is calibrated based on experimental data from a PMO population. The anabolic action of PTH is considered via an administration dependent (i.e., a negative sigmoidal regulatory function) of the apoptosis rate of active osteoblasts. The latter is controlled via 3 ODE's describing intracellular signaling. Mechanical feedback is implemented using a characteristic time scale of days to weeks. The proposed model has been calibrated on clinical data showing BMD changes at different bone sites (femoral neck: FN and lumbar spine: LS) after a 2 years treatment with 20 μg of PTH (1-34) given daily and subcutaneously ^c. Habitual mechanical loading is set such as to obtain a physiological strain of 800 $\mu\epsilon$ on each bone site.

RESULTS

We compared the relative changes in bone matrix volume fraction (Δf_{bm}) resulting from a daily injection of 20 μg of PTH (1-34) with the experimental data from Leder et al. ^c (Figure 1). We obtain a site-specific bone gain of 8.8% ($9.4 \pm 1.13\%$) at the LS and 3.2% ($2.82 \pm 0.72\%$) at the FN. Bone gain depends nonlinearly on administration dose giving respectively 0.7%, 3.4% and 7.5% for 10, 20 and 40 μg PTH at the femoral neck over a 2 years treatment. Superimposing mechanical disuse onto our simulation leads to a 3.2% reduction of bone gain at the FN over a 2 years treatment period.

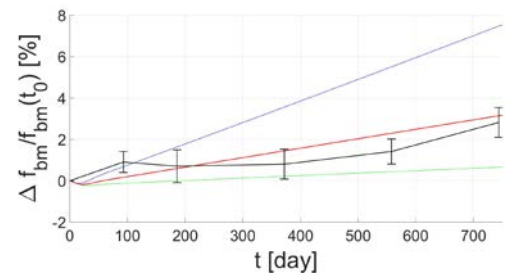


Figure 1. Relative changes of FN fbm during 2 years treatment with different daily-injected doses of PTH (1-34): 10 μg (green), 20 μg (red), and 40 μg (blue). Black curve: experimental data and error bars from Leder et al. ^c

CONCLUSIONS

The developed mechanistic PK/PD model of PTH (1-34) treatment of PMO is novel in several ways: (i) it includes calibrated PK data for women with PMO and (ii) it utilizes a mechanobiological feedback in the bone remodeling model. The numerical simulations show good agreement with experimental data. Bone gain is nonlinearly dependent on PTH dose and bone site. Interestingly, our model predicts that patients with reduced daily activity respond less to PTH treatment. While animal experiments support his finding, further experimental data is required in humans.

REFERENCES

- a : Trichilo et al., JOURNAL'S NAME, 2018
- b : Scheiner et al., CMAME 254:181-196, 2013
- c : Leder et al., JCEM 99(5):1694–1700, 2014

CAN HUMERAL FRACTURES OCCUR SPONTENIOUSLY IN INFANT WHILE ROLLING? A FINITE ELEMENT STUDY

Zainab Altai^(1,2), Marco Viceconti^(1,2), Amaka C Offiah^(1,3), Xinshan Li^(1,2)

1.INSIGNEO Institute for in silico medicine, The University of Sheffield, UK; 2. Department of Mechanical Engineering, The University of Sheffield, UK; 3. Department of Oncology and Human Metabolism, The University of Sheffield, UK

INTRODUCTION

Humeral fractures are common during childhood. However, for infants with limited ambulation, these are suspicious for child abuse in the absence of an appropriate history of trauma. A possible accidental mechanism has been previously reported by Hymel and Jenny in 1996¹, in which they proposed that a humeral fracture might occur when infants are rolled from prone to supine with their arm trapped behind their body by an external force. A recent study in 2014 reported seven cases of humeral fracture, initially described as “non-accidental injuries”, and suggested all 7 resulted from the Hymel mechanism². However, unlike the Hymel report, there was no external force acting on the body during the roll (i.e. these were spontaneous fractures). This has led to a debate in the clinical community. The aim of the current study is therefore to investigate the possibility of a spontaneous humeral fracture when rolling from prone to supine using a CT-based finite element modelling approach³.

METHOD

Three post-mortem CT scans (two 4-month-old and one 6-month-old infant) were used. The left humerus of each child was segmented in ITK-SNAP and meshed in ICEM 16.1 (Ansys INC., PA, USA) using 10 node tetrahedral elements. It was assumed that the humerus was subjected to the infant’s body weight, therefore, the rotational load needed by each child to roll to supine position (Figure 1) was calculated and applied at the proximal end of the humerus FE model. The boundary conditions were selected to represent a trapped humerus underneath the trunk (Figure 2).

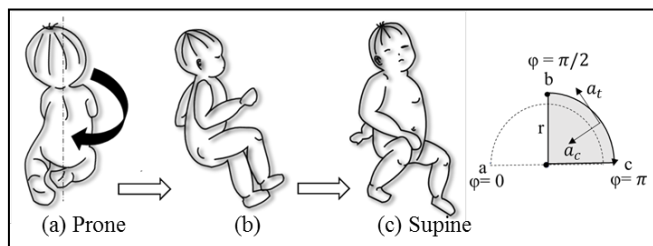


Figure 1. Sketch of an infant rolling from prone to supine with one arm positioned behind the body.

Sixteen various orientations of the arm during the roll were simulated (0-60° and 0-45° degrees in vertical and horizontal extensions, respectively). Maximum tensile and compressive principal strains were predicted for each case and compared against the elastic limit of the adult human bone (0.73% in tension and 1.04% in compression)⁴.

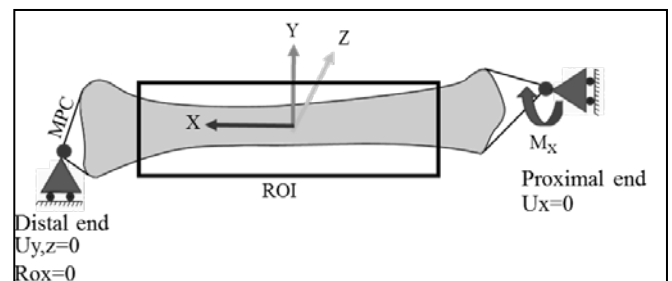


Figure 2. Schematic of the humerus FE model.

RESULTS

The maximum first principal strains for the sixteen simulated orientations were 0.113% and 0.108% for the 4-month-old and 0.139% for the 6-month-old. The highest predicted strains were substantially lower (with a difference of more than 80%) than the elastic limit of human bone. The highest strains were predicted at either the middle or towards the distal end of the humeral shaft.

CONCLUSIONS

The results of the simulations show that it is highly unlikely for the bone to fail spontaneously, given the underlying modelling assumptions. In order to confirm this finding, further investigation is required, including more cases with more accurate boundary conditions established for the rolling maneuver.

REFERENCES

1. Hymel, PK. Arch Pediatr Adolesc Med 150, 226-228, 1996.
2. Somers, JM. Pediatr Radiol 44, 1219-1223, 2014.
3. Altai, Z. Biomech Model Mechanobiol 2018.
4. Bayraktar, HH. J Biomech 37, 27-35, 2004.

Zainab Altai
Zakaltai1@sheffield.ac.uk

TIME-COURSE CHANGES OF LOWER LIMB KINEMATICS DURING MILITARY LOAD-CARRIAGE

Jodie A. Wills¹, David J. Saxby², Gavin Lenton², Timothy L. A. Doyle¹

Faculty of Medicine and Health Sciences, Macquarie University, Sydney, Australia¹
Menzies Health Institute Queensland, Griffith University, Gold Coast, Australia²

INTRODUCTION

Occupational physical employment performance standards require soldiers to carry loads >20kg. Increased physical demands of loaded walking result in variations of lower limb kinematics and mechanical work [1]. To efficiently meet task demands, hip joint contributions increase to assist forward progression [2]. Quantification of lower-limb kinematics over an extended duration loaded walking task will help provide further understanding of how task demands are met. This study examined how lower-limb gait kinematics differed before and after a loaded walking task.

METHOD

Fifteen male civilians participated within this study (age 22.4 ± 1.6 years, height 1.82 ± 0.06 m, body mass 83.8 ± 6.7 kg). At the time of testing, no participants had acute or chronic injuries. No former experience with load-carriage was required. Participants gave written informed consent to the protocol and Macquarie University Human Research Ethics Committee approved the study (protocol number: 5201700406). Participants were required to meet or exceed the Army Basic Fitness Assessment (BFA) standards for male soldiers ≤ 25 years old [3] (70 sit-ups and 40 push-ups in 2 minutes each), body mass ≥ 73 kg, and have a maximal aerobic capacity ≥ 45 mL·kg⁻¹·min⁻¹.

A single treadmill load-carriage task representative of the minimum Australian Army All Corps physical employment standard (5 km at 5.5 km·h⁻¹, wearing a 23 kg vest) was completed. Three-dimensional motion capture and over-ground force plate data were acquired for ten successful over-ground loaded walking trials pre and post the 5 km task (defined as: 1) the participant strikes the force plate cleanly, 2) walking speed equates to 5.5 km·h⁻¹ \pm 0.1%). A scaled full-body OpenSim model was used to estimate hip, knee, and ankle joint angles from inverse kinematics. Data was compared before and after the assigned loaded walking task.

Paired samples t-tests were conducted on all variables. Significance was set at $p < 0.05$. Effect sizes were calculated using difference in means (d) and were interpreted as trivial, small, moderate, and large effects

for values of d equal to 0.0, 0.2, 0.6, and 1.2, respectively [4].

RESULTS

Results are presented for eight participants; the remaining seven participants data are currently being analysed. Significant increases in peak hip extension ($t(7) = 3.805$, $p = 0.007$, $d = -0.56$), hip abduction ($t(7) = -2.864$, $p = 0.024$, $d = 0.51$) and knee flexion angle ($t(7) = -4.496$, $p = 0.003$, $d = 0.03$) values were demonstrated after the loaded walking task. Peak knee extension angle significantly decreased ($t(7) = 2.603$, $p = 0.035$, $d = -0.21$). Trivial-to-moderate effect sizes were shown for peak joint variables.

Table 1. Mean \pm standard deviation of gait kinematics.

* indicates a significant difference between pre-post walking variable values ($p < 0.05$).

Variable	Walking Condition		Significance <i>P</i> -value	Effect Size <i>d</i>
	Pre	Post		
Stride length	1.62 \pm 0.04	1.62 \pm 0.03	.963	0.02
Step width	0.07 \pm 0.03	0.06 \pm 0.023	.240	-0.26
Peak hip extension angle	-19.36 \pm 2.70	-20.95 \pm 3.01	.010*	-0.56
Peak hip flexion angle	34.23 \pm 6.64	33.20 \pm 6.16	.166	-0.16
Peak hip abduction angle	11.72 \pm 2.49	12.88 \pm 2.02	.024*	0.51
Peak hip adduction angle	-15.44 \pm 4.99	-15.27 \pm 5.24	.737	0.03
Hip angle at heel strike	32.55 \pm 6.41	31.55 \pm 6.00	.114	-0.16
Peak knee extension angle	2.75 \pm 2.90	2.18 \pm 2.55	.035*	-0.21
Peak knee flexion angle	70.26 \pm 4.39	71.53 \pm 4.12	.003*	0.30
Knee angle at heel strike	9.38 \pm 2.09	9.91 \pm 2.60	.320	0.22
Peak ankle dorsiflexion angle	9.49 \pm 3.51	7.96 \pm 4.02	.354	-0.41
Peak ankle plantarflexion angle	-20.66 \pm 7.89	-22.35 \pm 5.86	.324	-0.24
Ankle angle at heel strike	2.99 \pm 2.87	1.63 \pm 4.63	.331	-0.35

CONCLUSIONS

Current findings support previous results reported within load-carriage literature. Investigating the effects of an evidence-based physical training intervention will enable further understanding of time-course changes in lower-limb kinematics.

REFERENCES

1. Huang, T. (2014). *J Exp Biol*, 217, 605–613.
2. Lenton, G. (2017). *J. Sci. Med. Sport*, 20, S106.
3. Mullins, A.K. (2015). *Ergonomics*, 58, 770-780.
4. Hopkins, W. (2016). Available from: <http://www.sportsci.org/resource/stats/effectmag.html>.

SPEAKER INFORMATION

Speaker: Jodie A. Wills

Email: Jodie.wills@hdr.mq.edu.au

DEVELOPMENT OF A DEEP NEURAL NETWORK FOR AUTOMATED ELECTROMYOGRAPHIC PATTERN CLASSIFICATION

^{1,2}Riad Akhundov, ¹Laura E Diamond, ²Suzi Edwards, ³Suzanne Snodgrass, ⁴Phil Clausen, ¹David J Saxby

¹School of Allied Health Sciences, Griffith University, Australia, ²School of Environment and Life Sciences, University of Newcastle, Australia, ³School of Health Sciences, University of Newcastle, Australia, ⁴School of Engineering, University of Newcastle, Australia

INTRODUCTION

Neuromusculoskeletal modelling can be used to estimate muscle dynamics and simulate human biomechanics [1]. The Calibrated EMG-informed Neuromusculoskeletal Modelling toolbox (CEINMS) [2] is a software framework for neuromusculoskeletal modelling, which uses experimental measures of electromyographic (EMG) activity to calculate in vivo joint forces and joint moments.

Recordings of EMG can have a low signal to noise ratio that makes any interpretation of these muscle activations challenging. These EMG signals must contain clear bursts of activity associated with muscle activation during motor tasks in order to be used in CEINMS or other neurophysiology applications. As such, the quality of experimental EMG data must be assessed in order to verify its validity and utility for use in neuromusculoskeletal modelling.

The manual evaluation of the EMG data quality is time demanding and subjective. Development of an automated process that determines EMG quality could streamline EMG data processing. A useful solution for EMG data classification may be provided by neural networks that have gained popularity as a means of machine learning for classification. The aim of this study was to automate the EMG quality evaluation process using a neural network.

METHOD

Over 87,000 individual EMG signals from various lower limb muscles were used to train three neural network architectures with the goal of automatically classifying EMG quality. The three networks were: adaptive neuro fuzzy inference system (ANFIS); pattern recognition neural network (PNN); and convolutional neural network (CNN). The first two approaches (ANFIS & PNN) extracted coefficients to describe the EMG signal and used these coefficients as input for the neural network. These coefficients included wavelet transform, variance, spectral entropy and other features that are generally used for pattern classification [3]. The third approach (CNN) implemented a deep neural

network that extracted coefficients from the input data without supervision. All three networks were trained by manually classified images of EMG signals (n=7000).

RESULTS

The neural network performance of both ANFIS and PNN was unsatisfactory (Table 1); accuracy (the percentage of correct classifications) was relatively low and false-positives rates (percentage of poor quality EMG falsely classified as good quality) were high.

Table 1. Accuracy and false-positive (%) of the neural network architectures.

Architecture	ANFIS	PNN	CNN
Accuracy	60.0%	70.9%	99.6%
False-positives	30.3%	15.9%	0.0%

ANFIS - adaptive neuro fuzzy inference system; PNN - pattern recognition neural network; CNN - convolutional neural network.

The neural network performance of the CNN resulted in a significant improvement in classification accuracy that was high enough to effectively eliminate any false-positives. These preliminary results suggest that a deep neural network may be effective for automated EMG classification. The implementation of all available data is ongoing. Once complete, we aim to build a classification tool and make it publicly available.

CONCLUSIONS

Using an image recognition-based deep neural network, the quality of EMG signals can be successfully classified as good, usable or poor. Findings from this study will underpin a classification tool designed to save researchers time and eliminate human errors when subjectively processing experimental EMG data.

REFERENCES

- [1] Buchanan et al., J Appl. Biomech. 20(4), 367–395, 2004.
- [2] Pizzolato et al., J Biomech. 48(14), 3929–3936, 2015.
- [3] Phinyomark et al., El. and El. Engin. 6(122), 1215–1392, 2012.

Riad Akhundov - r.akhundov@griffith.edu.au

HIP ARTHOKINEMATICS DETERMINED USING SUBJECT-SPECIFIC MRI AND MESH CONTACT THEORY

David J Saxby¹, Edin Suwarganda¹, David G Lloyd¹, Laura E Diamond¹, Claudio Pizzolato¹

¹School of Allied Health Sciences, Griffith University, Gold Coast, Australia

INTRODUCTION

Abnormal femur and acetabulum bone morphology may cause abnormal hip kinematics seen femoroacetabular impingement syndrome patients [1]. We present an application of mesh contact theory [2] to determine the three-dimensional hip motion envelope, which defines all possible rotational motions constrained by rigid contact.

METHODS

Pelvis and femur bones from 4 healthy adults were acquired using 3T MRI (Ingenia, Phillips Healthcare, Netherlands). Images were manually segmented (Mimics v18, Materialise, Belgium), triangulated surface meshes were created [3], and anatomic coordinate systems embedded [4].

Hip motion envelope was determined by computationally mobilizing the digital hip through all possible combinations of 0-130° flexion (FE) and 0-90° adduction (ADD) (MATLAB, Mathworks, USA). For each FE and ADD pose, internal rotation (IR) angle causing femoroacetabular contact was determined with a binary search strategy using an efficient mesh contact detector [2]. Minimum step size on the binary search was set to the MRI resolution.

Hip motion envelope (Fig-1A), maximum rotational motion toward impingement (largest sum of FE, ADD, and IR), maximum pure rotations (FE, ADD, and IR), and maximum individual and combined ADD and IR at 90° FE are reported.

RESULTS

Hip motion envelope has conic shape (Fig-1A), and an irregular surface indicating complex patterns of impingement. As FE and ADD increase, IR causing impingement decreases.

Table 1. Hip motion envelope parameters.

Max Rotations to impingement						
Total	FE	ADD	IR	Max Pure FE	Max Pure ADD	Max Pure IR
140.1±4.2°	75±44°	23±20°	49±31°	118±24°	77±6.7°	90°*

*Pure internal rotation does not cause impingement in bounds tested.

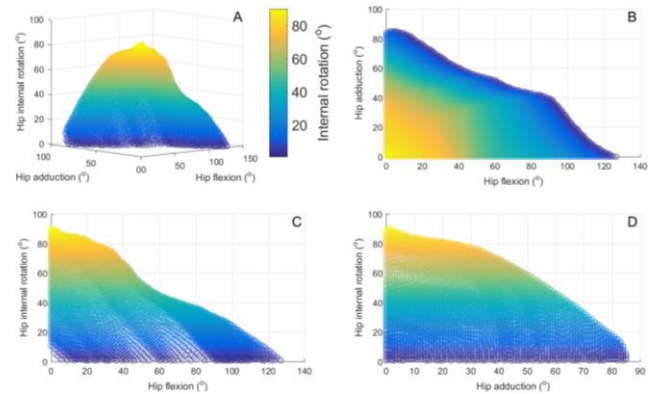


Fig-1. (A) Internal rotation angle where femoroacetabular contact occurred against all combinations of 0-130° flexion and 0-90° adduction. (B) Adduction and flexion, (C) internal rotation and flexion, and (D) internal rotation and adduction.

CONCLUSIONS

This, the first report of the hip motion envelope (Fig-1) from subject-specific MRI, revealed maximum motion into impingement and pure rotations larger than literature reports from hip pathology patients [1,5], indicating morphologic abnormalities femoral and acetabular components reduce the hip movement envelope. Our method may enable differentiation of pathologic from healthy hips, without physical exam or x-ray-based diagnostics. We present preliminary findings, but will extend analysis to pathological populations to determine clinical utility.

REFERENCES

1. Kapron, A. L., et al. J Biomech 48, 2879-2886, 2015.
2. Moller, T. J Graph Tools, 2, 25-30, 1997.
3. Zhang, J., et al. Biomed Sim, Springer, 182-192.
4. Wu, G., et al. J Biomech, 35, 543-548, 2002.
5. Kobayashi, N., et al. Arthroscopy, 33, 329-334, 2017

David John Saxby, d.saxby@griffith.edu.au

ABC 11 - Program – DAY 2

Lecture theatre 505-011, Grafton Campus

4th Dec 2018

<p style="text-align: center;">3.30 pm to 5.15 pm</p> <p style="text-align: center;">Session Chairs: Dr Fatemeh Malekipour and Dr Kelly Wade</p>	<p>COMPUTATIONAL MODELING II</p> <p>Invited Speaker - Dr Alys Clarke</p> <p>University of Auckland/ Auckland Bioengineering Institute</p> <p>On: BIOMECHANICS OF PREGNANCY: FROM CONCEPTION TO DELIVERY</p> <p>Scientific Presentations</p> <ul style="list-style-type: none"> • Biomechanical role of anterolateral ligament in ACL-deficient knee: a 3D finite element study - Duraisamy Shriram (Singapore University of Technology and Design) • Image-driven Modelling and Simulation of Micro-scale Articular Cartilage Mechanics - Scott Sibole (University of Calgary) • Identifying the unloaded shape and stiffness of the breast - Thiranjia Prasad Babarenda Gamage (University of Auckland) • How to estimate the friction coefficient of articular cartilages using in-vivo imaging of the joints? - Saeed Miramini (University of Melbourne) • Rapid prediction of personalized achilles tendon tissue strains with a machine learning technique – Vickie Shim (University of Auckland) • Influence of the reference state on estimators of cardiac contractility – Mario Habenbacher (Graz University of Technology)
--	---

BIOMECHANICAL ROLE OF ANTEROLATERAL LIGAMENT IN ACL-DEFICIENT KNEE: A 3D FINITE ELEMENT STUDY

Duraisamy Shriram¹, Gideon Praveen Kumar², Fangsen Cui², Yee Han Dave Lee³, Karupppasamy Subburaj¹

¹Engineering Product Development Pillar, Singapore University of Technology and Design, Singapore;

²Institute of High Performance Computing, A*STAR, Singapore; ³Department of Orthopaedic Surgery, Changi General Hospital, Singapore.

INTRODUCTION

The anterolateral ligament (ALL) has been proposed as a secondary restraint to control tibial translation and rotation. Unaddressed injury to the ALL in the anterior cruciate ligament (ACL) reconstructed knee joint may result in subtle mechanical instability (Parsons *et al.*, 2015). Given the recent advancements in understanding the anatomy, histology, and incidence of the ALL (Vincent *et al.*, 2012), the biomechanical role of this ligament in the knee joint kinematics and its clinical implications have not been fully delineated. Thus, the aim of this study was to investigate the biomechanical role of sectioning the ALL in the ACL-deficient knee. We hypothesized that there would be a significant change in the tibial anterior-posterior translation and rotational instability during the normal walking gait in the presence of ALL lesion in the ACL-deficient knee.

METHOD

Magnetic resonance (MR) image acquisition of the left knee of a healthy volunteer (gender: male, age: 29 years, BMI: 23 kg/m²) was performed with a 3-Tesla GE Signa HDx MR scanner. A three-dimensional finite element (FE) model of the knee joint was developed using the structures segmented from MR images of the knee joint. The ligaments and the menisci were modelled as hyperelastic transversely-isotropic material (Holzapfel-Gasser-Ogden model). Cartilages were defined as hyperelastic isotropic non-linear material (neo-Hookean model). Cartilages, ligaments, and the menisci were meshed using quadratic tetrahedron type elements. FE simulations were conducted on the knee joint model for the following cases: (i) intact joint, (ii) ACL resection, and (iii) combined ACL and ALL resection.

RESULTS

ACL resection significantly increased the tibial anterior-posterior translation during the main events of the gait cycle (Figure 1a). Significant changes in the tibial internal-external rotation were estimated in the ACL-deficient knee during the initial contact, toe off, and the tibia vertical events of the gait cycle (Figure 1b). ALL resection significantly increased the tibial translation and rotation at all main events of the gait cycle (Figure 1a-b) in the ACL-deficient knee joint. Considering the absolute values of tibial translation and rotation, the peak values were observed in the knee joint model with combined ACL and ALL resection.

CONCLUSIONS

ALL resection in ACL-deficient knee increased the tibial anterior-posterior translation and interior-exterior

rotation. These findings make it clear that injuries to the ALL have a clinical impact on joint stability and highlight the significance of ALL as the extra-articular stabilizer of the knee. This computational model will serve as a decision aid for clinicians to assess the anterolateral aspect of the knee when facing an ACL reconstruction in the endeavor to obviate residual instability of the knee.

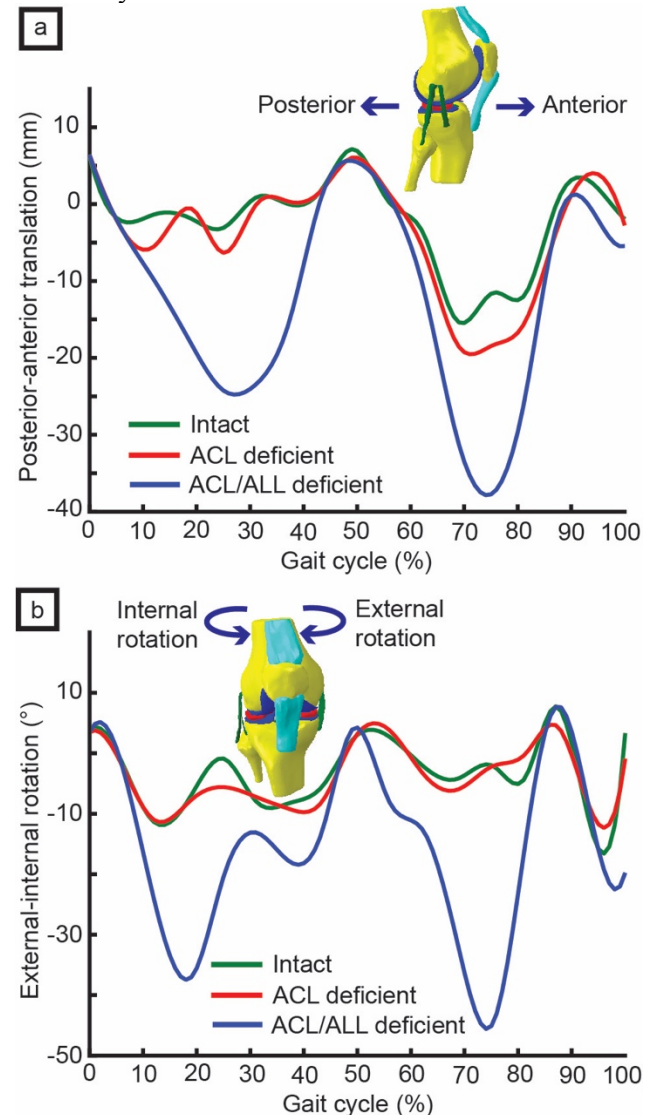


Figure 1. (a) Tibial anterior-posterior translation and (b) tibial external-internal rotation of the intact, ACL deficient, and combined ACL/ALL deficient knee joint

REFERENCES

- 1) Parsons, E. M. *et al.* Am J Sports Med 43, 669-674, 2015.
- 2) Vincent, J. P. *et al.* Knee Surg Sports Traumatol Arthrosc 20, 147-152, 2012.

Speaker Name: Duraisamy Shriram

Email ID: shriram_duraisamy@mymail.sutd.edu.sg;
shriram@biomechresearch.com

IMAGE-DRIVEN MODELLING AND SIMULATION OF MICRO-SCALE ARTICULAR CARTILAGE MECHANICS

Scott C. Sibole¹, Eng Kuan Moo¹, Salvatore Federico^{1,2}, Walter Herzog¹

1. Human Performance Laboratory, University of Calgary, Calgary, Canada

2. Mechanical and Manufacturing Engineering, University of Calgary, Calgary, Canada

INTRODUCTION

We recently introduced a method to determine the three-dimensional (3D) kinematics of deforming articular cartilage (AC) at the micro-scale level using a multiphoton laser scanning microscope in conjunction with a mechanical testing system¹. The technique involves the photobleaching of a 3D grid onto the tissue, which provides trackable features allowing for accurate and robust deformable image registration. The measurement of these micro-scale kinematics unveils many potential avenues for additional investigation. One such avenue is to employ the image data and kinematics to define boundary value problems of tissue subregions. The images can provide pointwise material information and the displacement boundary conditions can be assigned directly from the measured kinematics. The boundary value problem can then be solved numerically, e.g., via the Finite Element (FE) Method. In this study, we demonstrate such a procedure informed by the grid-marked images and an additional image acquired in the reference configuration using second harmonic generation (SHG). SHG allows for measurement of local type II collagen content and fibre orientation allowing the collagen-dependent material properties to be directly mapped from image to model.

METHOD

3D kinematics were determined for porcine AC under 30% nominal strain at steady state. An SHG image was also acquired in the reference configuration. The image-based simulation technique is briefly outlined as follows. 1) A coherence enhancing anisotropic diffusion filter² was applied to the SHG image to reduce noise and enhance aligned features (Figure 1A). 2) Ellipsoidal probability density functions (PDFs) of collagen orientations were determined based on the eigenvalues and eigenvectors of the Hessian of the image intensities at each voxel.³ 3) FE meshes were defined in a region of the superficial zone containing a cluster of cells. 4) The PDFs and intensities were linearly interpolated from the image voxels to the centroids of the elements (Figure 1B). 5) Material properties were defined for each element based on these intensities and PDFs. 6) Displacement boundary conditions were determined and assigned by applying the transform calculated from the image registration to each model surface node. 7) To investigate the effect of collagen anisotropy, a second model was generated

for the same region but all PDFs were replaced by spheres, reflecting isotropy in the reference configuration. 8) Solutions were obtained with FEBio v2.5.⁴

RESULTS AND CONCLUSIONS

While this was intended as a proof of method study, notable differences were observed between the referentially isotropic (Figure 1C) and anisotropic model (Figure 1D). The first (maximum) principal stress fields differed between cases in both magnitude and direction. The image-based anisotropic model had lower stresses in the cellular regions. Although the referentially isotropic model does not have an initial preferred direction, clear patterns arise during deformation. Conclusions, however, cannot be drawn from a single specimen. Nevertheless, further experimentation and simulation studies employing the demonstrated technique may provide valuable insight into these cellular scale mechanical questions.

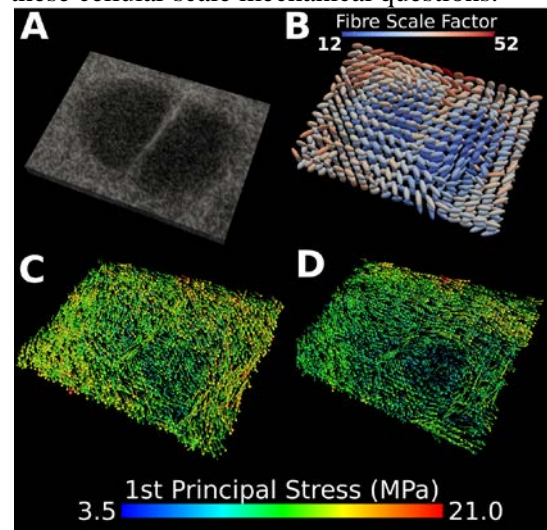


Figure 1. A) The modelled region of the SHG image after filtering. B) The PDFs of collagen fibre orientation mapped to the finite element centroids. C) The 1st principal stresses calculated for the referentially isotropic and D) anisotropic models.

REFERENCES

1. Moo, EK and Sibole, SC et al. *Acta Biomater* 70, 260-269, 2018.
2. Frangi AF et al. *Medical Image Computing and Computer-Assisted Intervention*. Springer 1998.
3. Weickert J et al. *Int J of Comput Vision* 31, 111-127, 1999.
4. Maas S et al. *J Biomech Eng* 134, 11005, 2012.

IDENTIFYING THE UNLOADED SHAPE AND STIFFNESS OF THE BREAST

Thiranja Babarenda Gamage¹, Alexander Catalinac², Duane Malcolm¹, Poul Nielsen^{1,2}, Martyn Nash^{1,2}

¹Auckland Bioengineering Institute, University of Auckland, New Zealand

²Department of Engineering Science, University of Auckland, New Zealand

INTRODUCTION

Breast cancer is the leading cause of cancer-related death in females, affecting 1 in every 10 women worldwide. Clinical imaging modalities used for diagnosing the disease, such as prone diagnostic magnetic resonance imaging (MRI), are acquired with the patient positioned differently to that assumed during breast conserving treatment procedures, which are performed in a different position (e.g. supine). This makes it difficult for clinicians to locate and excise tumours. We have developed an automated clinical pipeline that constructs biomechanical models from diagnostic prone MRI and predicts tumour motion during treatment procedures (Figure 1).

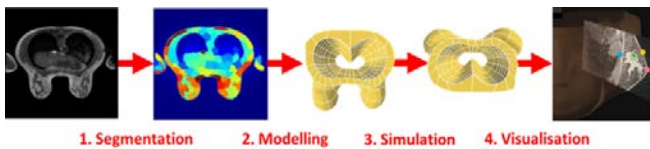


Figure 1. Clinical pipeline for predicting tumor motion from the prone position to the supine position.

The individual specific stiffness and the gravity-free unloaded configuration of the breast are required for accurate model predictions. The results from state of the art techniques for estimating these parameters are dependent on the gravity loaded configuration that is used to construct the model (e.g. from either diagnostic prone MRI or an additional MRI acquired in the supine position). This can produce biased parameter estimates and inaccurate model predictions of tissue motion. This study aimed to develop and verify a novel framework for simultaneously identifying the unloaded configuration and stiffness of the breast from multiple loaded configurations.

METHOD

Our clinical pipeline was used to construct breast models from prone MR images of 54 volunteers. An existing numerical algorithm [2] was used to determine the unloaded configuration using 4 representative neo-Hookean breast stiffness parameters for each volunteer. A principal component analysis (PCA) was performed on the resulting population of unloaded configuration shapes. To facilitate verification of the framework, only the first principal shape component (PC 1) accounting for 57.3 % of the observed shape variation in the unloaded configuration was retained. The prone and supine shapes were then

simulated from the reduced PCA model of each volunteer and stiffness parameter considered (216 cases) and were treated as synthetic data in subsequent analyses. A verification analysis was performed to determine if the first principal shape component of the unloaded configuration and stiffness could be correctly recovered from the synthetic data. This was achieved for each case using an optimization procedure to simultaneously tune the first principal shape component of the unloaded/reduced PCA population model to minimize differences between the predicted prone and supine shapes and their corresponding target shapes observed in the synthetic data.

RESULTS

Biased estimates of the unloaded shape and stiffness were obtained when the parameters were identified from either prone or supine loaded configurations, while robust parameter estimates were obtained when parameters were identified from both configurations (Figure 2).

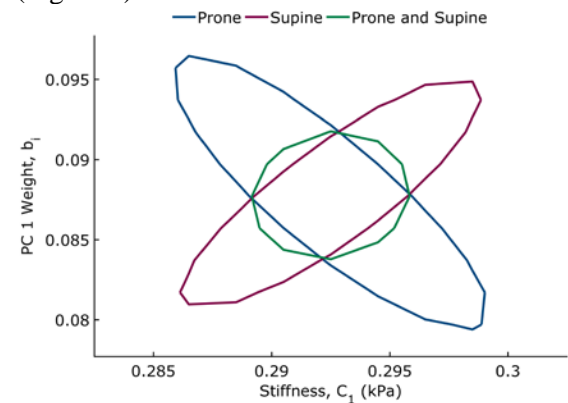


Figure 2. Representative prediction error contour plot for a volunteer case indicating the valid range of shape and stiffness parameters that can be identified from only prone or supine loaded configurations, and their combination.

CONCLUSIONS

The framework was verified using synthetically generated prone and supine shape data. The framework will be validated in future work using prone and supine shape data from MR images.

REFERENCES

- [1] Annals of Surgical Oncology. 16(10), 2717-2730, 2009.
 - [2] Int J Numer Method Biomed. 72(12), 1434-51, 2007.
- Thiranja Babarenda Gamage, psam012@aucklanduni.ac.nz

HOW TO ESTIMATE THE FRICTION COEFFICIENT OF ARTICULAR CARTILAGES USING IN-VIVO IMAGING OF THE JOINTS?

¹ Saeed Miramini, ²David W Smith, ¹Lihai Zhang and ³Bruce S Gardiner

¹Melbourne School of Engineering, The University of Melbourne, VIC

²Faculty of Engineering, Computing and Mathematics, University of Western Australia, WA

³School of Engineering and Information Technology, Murdoch University, WA

INTRODUCTION

Articular cartilage tissue can be considered as a biphasic material composed of a highly porous solid matrix saturated with interstitial fluid. Under compressive loading, the interstitial fluid gradually leaves the solid matrix and drains through the cartilage surface, resulting in a time-dependent tissue deformation known as consolidation. The experimental results suggest that the cartilage friction coefficient rises with loading duration [1], potentially leading to increased cartilage surface wear. In this study, we hypothesize that there should be a correlation between the cartilage friction coefficient and characteristic time for cartilage consolidation.

METHOD

To test this hypothesis, we computationally simulate the mechanical consolidation response of human tibial cartilage under static compressive loading. The computational model is developed based on our previously published poroelastic model of human knee cartilage under cyclic loading [2]. The model takes into account the tension-compression nonlinearity of the cartilage and also incorporates a non-linear compressive stiffness based on the deformation-dependent aggrecan concentration of cartilage tissue. In addition, it takes into account the dependency of the fluid permeability of cartilage on the aggrecan concentration. We adopted an axisymmetric geometry of lateral tibial plateau with a contact area of 500 mm² in the computational model of this study. It is assumed that a compressive loading equivalent to 2.6 standard bodyweight (i.e. 2.59×750 N) is applied on the knee, simulating the knee joint loading during one legged stance, with an equal distribution of the load between medial and lateral compartments of the knee. For model details (e.g. boundary conditions, etc.), refer to our recent paper [3]. The model calculates the time-dependent deformation and Degree of Consolidation (DoC) for the cartilage. The DoC at time t can be defined as: $\text{DoC}(t)=[w(t)-w(0)]/[w(\infty)-w(0)]$ where $w(t)$ is peak contact deformation at time t , $w(0)$ is the deformation immediately after loading application and $w(\infty)$ is the steady state deformation.

RESULTS

The model predicts a peak contact strain (maximum vertical deformation divided by cartilage thickness) of

10% and 13.8% respectively 5s and 300 s after loading application, with a steady state contact strain of 25%. The model predictions have a good agreement with experimental measurements [4, 5]. To test the hypothesis of this study, in Figure 1, we plot both our computational result of DoC of the cartilage and Forster, et al's experimental measurement of friction coefficient of cartilage following application of static loading [1]. It can be seen that there is a strong linear positive correlation between DoC and friction coefficient at the joints suggesting that the DoC can be used as an index to evaluate the friction coefficient and the likelihood of cartilage surface wear [3].

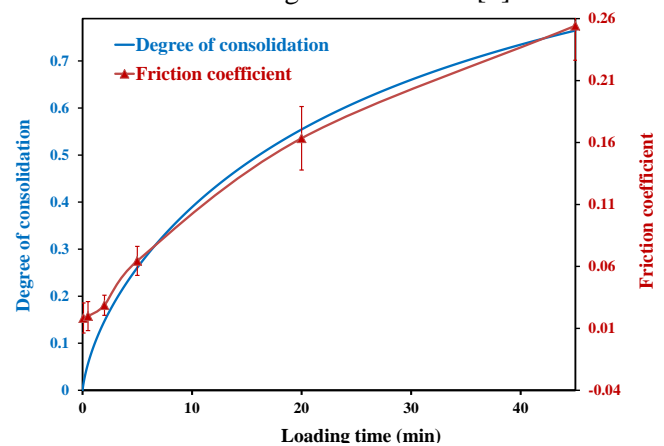


Figure 1. A strong correlation exists between the cartilage DoC and friction coefficient between opposing cartilage surfaces.

CONCLUSIONS

The results suggest that we can estimate the friction coefficient of cartilages by medical imaging of the degree of joint space closure over time (i.e. DoC vs time) and non-invasively assess the joint articulation health in clinical practice [3].

REFERENCES

1. Forster H, et al. *Proceedings of Inst Mech Eng H*. **210**:109-119, 1996.
2. Zhang L, et al., *Ann Biomed Eng*. **43**:1166-1177, 2015.
3. Miramini S, et al., *J Mech Behav Biomed Mater*. **74**:1-10, 2017.
4. Hosseini A, et al., *Osteoarthritis Cartilage*. **18**:909-916, 2010.
5. Barker M, et al., *Rheumatology*. **40**:274-284, 2001.

RAPID PREDICTION OF PERSONALIZED ACHILLES TENDON TISSUE STRAINS WITH A MACHINE LEARNING TECHNIQUE

Vickie B. Shim¹, Claudio Pizzolato², Thor F. Besier¹, Rod S. Barrett¹, David G. Lloyd²

¹Auckland Bioengineering Institute, University of Auckland, Auckland, New Zealand

²GCORE, Menzies Health Institute Queensland, Griffith University, Gold Coast, Australia

1

INTRODUCTION

Achilles tendon injuries are common, occurring about 250,000 per year in the US alone, yet the mechanisms of tendon injuries and degeneration remain unknown. Recent studies have indicated that the nature of tendon deformation, specifically heterogeneous strain distributions, may contribute to the development of overuse injuries and tendinopathy[1]. One of the most widely used method of characterizing tendon strain distribution is to use subject-specific finite element (FE) models[2]. Despite increases in high performance computing, however, complex finite element models are limited to small subject numbers. In order to translate computational tools to medical applications and large-scale visualisation, population-based models are a possible way forward. This concept uses the idea that large sets of pre-computed or measured data can train a model using machine learning or multivariate regression methods. In this study we present a novel coupling between continuum mechanics simulations and partial least squares regression (PLSR). We report accuracy associated with rapid prediction of tendon shape and strain.

METHOD

We have used the results from our previous study [2] where we analyzed the tendon internal strain patterns with subject-specific FE models. Our models have both geometry and tissue internal structure in the form of embedded fibres [3]. Results from these studies were used in our Partial Least Squares Regression(PLSR) model. We trained a PLSR model by simulating 30 scenarios (6 different tendon lengths for 5 different tendon fascicle torsion angles) from FE predicted models. PLSR creates a linear model to predict response variables from predictor variables. In this study, the predictor variables are tendon length and torsion angle, and the response variables are FE predicted stresses, deformed shape and tissue strain. Model accuracy was assessed by doing a ‘leave-one-out’ analysis where one simulation from 36 was left out of the PLSR model and predicted independently. This was repeated for each case to report an average error. We used the PLSR plugins given in the Python SciPy (www.scipy.org) and scikit-learn (machine learning) modules and these methods are encapsulated in the Musculoskeletal Atlas

Project, an open source toolkit for musculoskeletal model development (<https://simtk.org/projects/map>).

RESULTS

As shown in Figure 1, our PLSR model was able to predict tendon internal stress distribution with the RMS error of less than 7 MPa (which is less than 5% of the maximum stress).

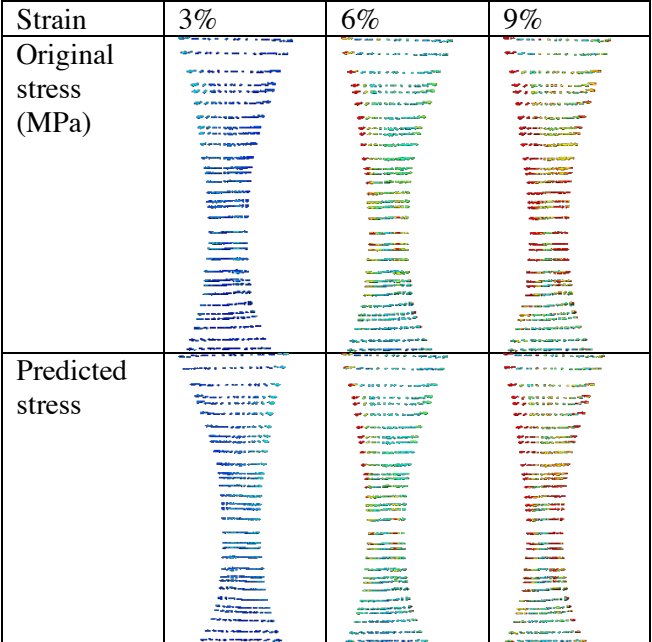


Figure 1. Comparison between original stress pattern and the predicted stress pattern from PLSR model (range 0-100MPa)

CONCLUSIONS

We have shown that our PLSR model was able to predict tissue internal stress pattern with a reasonable accuracy. This will be used in our personalized Achilles tendon treatment program as a real time predictor of internal tendon stress to identify subjects who are at risk for tendon rupture[4].

REFERENCES

1. Magnusson, S. P et al. *J Physiol* **586**, 71-81, doi:10.1113/jphysiol.2007.139105 (2008).
2. Shim, V. et al. *J. Biomech* **47**, 3598-3604
3. Shim, V. et al. Scientific Reports (in review)
4. Pizzolato et al. *BJSM* (accepted)

v.shim@auckland.ac.nz

INFLUENCE OF THE REFERENCE STATE ON ESTIMATORS OF CARDIAC CONTRACTILITY

Mario E. Habenbacher ¹, Zhinuo J. Wang ², Prasad B. Gamage ², Vicky Y. Wang ², Alistair A. Young ^{2,3},
Gerhard A. Holzapfel ^{1,4}, Martyn P. Nash ^{2,5}

¹Institute of Biomechanics, Graz University of Technology, Austria; ²Auckland Bioengineering Institute, University of Auckland (UoA), New Zealand (NZ); ³Department of Anatomy and Medical Imaging, UoA, NZ;
⁴Faculty of Engineering Science and Technology, Norwegian University of Science and Technology, Norway;
⁵Department of Engineering Science, UoA, NZ

INTRODUCTION

Heart failure (HF) refers to a diseased state of the heart, whereby its pumping ability is not able to sufficiently match the demands of the body [1]. Although HF is associated with high morbidity and mortality [1], imposing a high burden on health care systems worldwide [2], treatment of HF remains inefficient for roughly half of the affected population [3]. In order to model and simulate the mechanics of the LV, a well-defined reference state is necessary. Various studies have assumed different time points during the diastolic phase of the cardiac cycle to be “load-free” (LF), or have used different methods to estimate a stress-free reference state [4].

In this study, we investigate the influence of the selected reference state on model-based estimates of myocardial contractility. Therefore, the difference between patient-specific models, based on the diastasis (DS) and an estimated LF geometry (method described in [5]) as defined reference states and for a fixed set of material parameters, is examined.

METHOD

This study includes HF and control subjects from the St. Francis Hospital Heart Centre (New York, USA). The clinical data comprises cine MRI as well as same-day catheter pressure recordings. LV models, consisting of 16 cubic Hermite finite elements (FE), were obtained by parameterising a semi-automated segmentation of the cine MRI throughout the cardiac cycle of each subject.

Passive properties of the myocardium were described via a transversely isotropic exponential constitutive model [6], and contractile mechanical properties were modelled using the steady-state Hunter-McCulloch-ter Keurs constitutive model (Equation 1) [7].

$$T_a = T_{Ca} [1 + \beta(\sqrt{I_{4f}} - 1)] \quad (1)$$

For one subject out of control, HF with reduced ejection fraction (HFrEF) and HF with preserved ejection fraction (HFpEF), a forward simulation from the DS until the end of systole (ES) was performed.

Material parameters were obtained from minimising the error between the predicted model and cine MRI, endo- and epicardial surfaces for each subject with the DS as reference state. The difference between the estimated LF and DS geometries was quantified by calculating the Euclidean distance for the endo- and epicardial surfaces.

RESULTS

In case of high DS pressure (e.g. hypertension) the difference between LF and DS geometry can be substantial, leading to variation for predicted geometries throughout the cardiac cycle (e.g. end-systolic geometry of HFrEF subject in Figure 1).

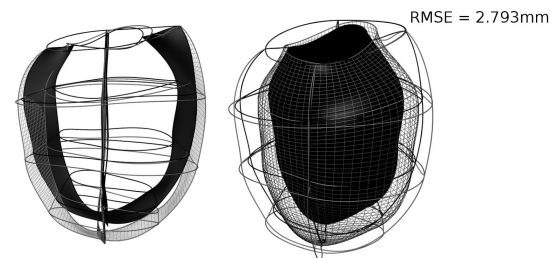


Figure 1: ES geometry from forward simulation for DS (grey/wireframe) and LF (black) as reference state for the HFrEF subject.

CONCLUSIONS

This study showed that the reference state influences the predicted geometry and thus can have an effect on estimators of material properties. Future investigations will focus on using this framework to determine the influence on estimated active properties of the heart.

REFERENCES

- [1] L. M. Buja and J. Butany, Academic Press, 2015.
- [2] C. Cook et al., Int. J. Cardiol., 171(3), pp. 368–376, 2014.
- [3] T. E. Owan et al., N. Engl. J. Med., 355(3), pp. 251–259, 2006.
- [4] Z. J. Wang et al., CMBE17, pp. 221–224, 2017
- [5] V. Rajagopal et al., Int. J. Numer. Meth. Eng., 72, pp. 1434–1451, 2007
- [6] J. M. Guccione et al., J. Biomech., 28(10), pp. 1167–1177, 1995.
- [7] P. J. Hunter et al., Prog. Biophys. Mol. Biol., 69(2), pp. 289–331, 1998

Presenter: Mario Habenbacher, mhabenbacher@student.tugraz.at